Supplementary Information

Two-dimensional Mineral $[Pb_2BiS_3][AuTe_2]$: High mobility Charge Carriers in Single-atom-thick Layers

Lei Fang[1,3], Jino Im[2], Constantinos C. Stoumpos[1,3], Fengyuan Shi[4], Vinayak Dravid[4], Maxime Leroux[3], Arthur J. Freeman[2], Wai-Kwong Kwok[3], Duck Young Chung[3], Mercouri Kanatzidis[1,3]

[1]Department of Chemistry, Northwestern University, Evanston, Illinois 60208, USA

[2]Department of Physics and Astronomy, Northwestern University, Evanston, Illinois 60208, USA

[3]Materials Science Division, Argonne National Laboratory, Argonne, Illinois 60439, USA

[4]Department of Materials Science and Engineering, Northwestern University, Evanston, Illinois 60208, USA

I. Atomic coordinates and Anisotropic displacement parameters of $[Pb_2BiS_3][AuTe_2]$

Table S1. Atomic coordinates ($\times 10^4$) and equivalent isotropic displacement parameters ($Å^2 \times 10^3$) for $[Pb_2BiS_3][AuTe_2]$. U(eq) is defined as one third of the trace of the orthogonalized U^{ij} tensor.

	x	y	z	U(eq)
Pb(1)	4209(1)	2500	3192(2)	38(1)
Au(1)	2500	2500	-39(2)	29(1)
Bi(1)	7500	2500	3497(3)	35(1)
Te(1)	3936(2)	-2500	-59(3)	33(1)
S(1)	4137(7)	2500	6183(10)	23(2)
S(2)	7500	2500	6340(14)	24(3)

Table S2. Anisotropic displacement parameters ($Å^2 \times 10^3$) for $[Pb_2BiS_3][AuTe_2]$. The anisotropic displacement factor exponent takes the form: $-2p^2[h^2 a^{*2} U_{11} + ... + 2 h k a^* b^* U_{12}]$

	U^{11}	U^{22}	U^{33}	U^{23}	U^{13}	U^{12}
Pb(1)	34(1)	24(1)	56(1)	0	-1(1)	0
Au(1)	26(1)	13(1)	47(1)	0	0	0
Bi(1)	31(1)	21(1)	54(2)	0	0	0
Te(1)	29(2)	23(1)	45(2)	0	2(1)	0
S(1)	23(5)	11(4)	33(5)	0	11(4)	0
S(2)	18(7)	21(6)	34(7)	0	0	0

II. Multiband effect and the violation of the Kohler's rule

Our magneto-transport characterizations and band structure calculations agree with the multiband nature of the electronic structure of $[Pb_2BiS_3][AuTe_2]$. Other experimental evidence comes from the Hall coefficient measurements and from Kohler's rule scaling.[S1] Figure S1(a) shows the temperature dependent ρ in zero field, which displays a slight upturn below 42 K. Figure S1(b) displays the temperature dependent Hall coefficient R_H. Coincidently, R_H exhibits similar temperature dependence with that of ρ. The temperature dependent R_H is a sign of multiband effect. Another evidence of the multiband electronic structure is the violation of Kohler's rule.[S4] Kohler' rule depicts a scaling law between magneto-resistance at different temperatures with normalized magnetic fields $\mu_0 H/\rho(0)$, where H and $\rho(0)$ represent the magnetic field and resistivity at zero field, respectively. This rule is generally held to metals with single species of charge carriers and is violated in the presence of multiple groups of carriers with different mobility.

Figure S2(a) and (b) delineate the magneto-resistance (MR) and a plot of Kohler's rule scaling, respectively. The MR cannot be scaled by the reduced magnetic fields $\mu_0 H/\rho_0$. The failure of Kohler's rule scaling strongly attests to the multiband nature of $[Pb_2BiS_3][AuTe_2]$.

Our experiments cannot rule out the presence of a charge density wave as a source of the resistance upturn.[S3, S4] The Fermi surface nesting between electron pocket and hole pocket, shown in Figure 3(c), may indicate charge density wave occurring. Moreover, given the 2D electronic structure, electron correlation in the $[AuTe_2]$ plane could be sufficiently strong to induce a metal-insulator transition. In-depth understanding of this resistance anomaly is beyond the scope of this study, we leave this question for future investigations.

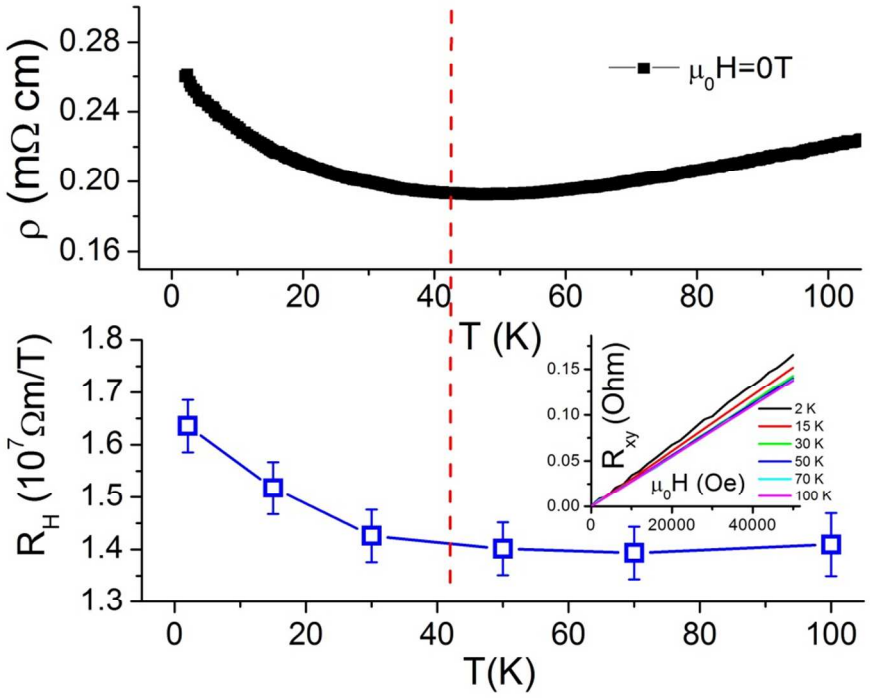

Figure S1. (a) Temperature dependent resistivity in zero fields. (b) Temperature dependent Hall coefficient measurements. The sign of the Hall coefficient is positive, indicating a hole-type carrier dominating the charge transport. This positive sign is consistent with our determination from the magneto-transport that the hole mobility is far greater than that of electron. The inset shows the field dependence of the Hall resistance.

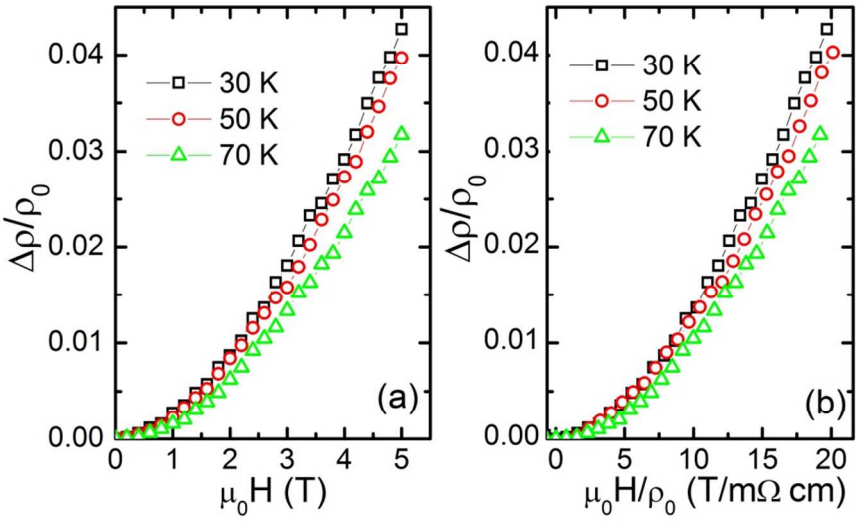

Figure S2. (a) Field dependent magneto-resistance (MR) of single crystal $[Pb_2BiS_3][AuTe_2]$ at different temperatures. (b) Attempted scaling of the MR data using Kohler's rule . MR at different temperatures cannot be scaled, indicating this material is a multiband metal.

III. Compensated two band model

The band structure of $[Pb_2BiS_3][AuTe_2]$ consists of one hole pocket and two electron pockets. The two electron bands have similar scattering process because of their identical Fermi surfaces. Therefore, the three band model can be simplified to a two band model which consists of one hole band and one electron band. Given the compensated density of the electrons and holes, the transport behavior of $[Pb_2BiS_3][AuTe_2]$ is determined by three parameters, the carrier concentration n_e=n_h, electron mobility μ_e and hole mobility μ_h.

The Hall resistance for the two band model [S4] is expressed as

$$\rho_{xy} = \frac{(R_e\rho_h^2+R_h\rho_e^2)B+R_eR_h(R_e+R_h)B^3}{(\rho_e+\rho_h)^2+(R_e+R_h)^2B^2} \quad \text{Equ. S1}$$

R_e and R_h are Hall coefficients of the electron band and hole band, respectively. R=1/ne, where n represents the carrier concentration and e is the charge unit. ρ_e and ρ_h are the resistivities of the electrons and holes, respectively. ρ=1/$ne\mu$, where μ denotes the mobility.

For a compensated two band model,

$$R_e\text{=-}R_h, \quad \text{Eq. S2}$$

and Eq.S1 can be simplified to

$$\rho_{xy} = \frac{(R_e\rho_h^2+R_h\rho_e^2)B}{(\rho_e+\rho_h)^2} \quad \text{Eq. S3}$$

The magnetoresistance of the two-band model is written as

$$\rho_{xx} = \frac{\rho_e\rho_h(\rho_e+\rho_h)+(\rho_eR_h^2+\rho_hR_e^2)B^2}{(\rho_e+\rho_h)^2+(R_e+R_h)^2B^2} \quad \text{Eq. S4}$$

For a compensated two band system, Eq. S4 reads

$$\rho_{xx} = \frac{\rho_e\rho_h(\rho_e+\rho_h)+(\rho_e R_h^2+\rho_h R_e^2)B^2}{(\rho_e+\rho_h)^2}$$ Equ. S5

Equ. S2, S3 and S5 are independent. Therefore, the three transport parameters, n_e (n_h), μ_e and μ_h can be directly solved from the three equations.

Figure S3 shows the temperature dependence of the mobility of electron and hole. This trend coincides well with the trend of the resistivity shown in Figure S1. The high hole mobility at 100 K may indicate an attractive feature for electronic applications.

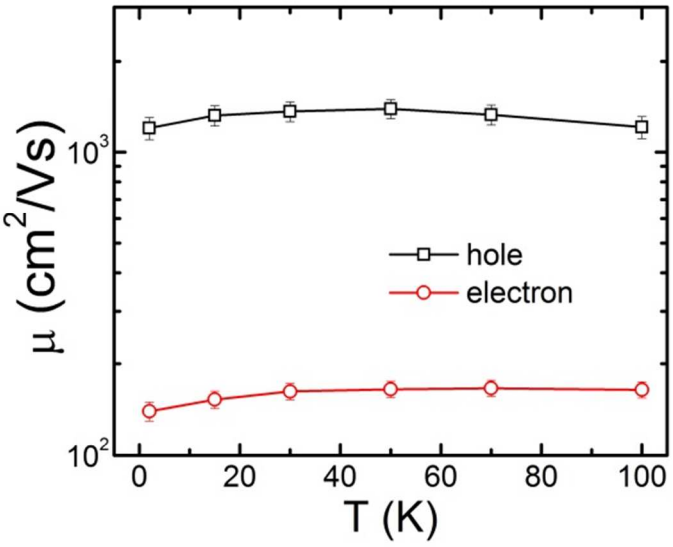

Figure S3. Temperature dependence of electron and hole mobility.

IV. Electronic coherency of the $AuTe_2$ layer

The chain-like structure in the [$AuTe_2$] layer is not considered to cause a periodic modulation of the in-plane electron density because of the covalent Te···Te bonds between chains, as revealed in our structure refinement. The existence of the Te···Te bond is also supported by our band structure calculations, which show significant exchange of the electron density between chains. Figure S4 is a plan-view of the electron density of the $AuTe_2$ layer.

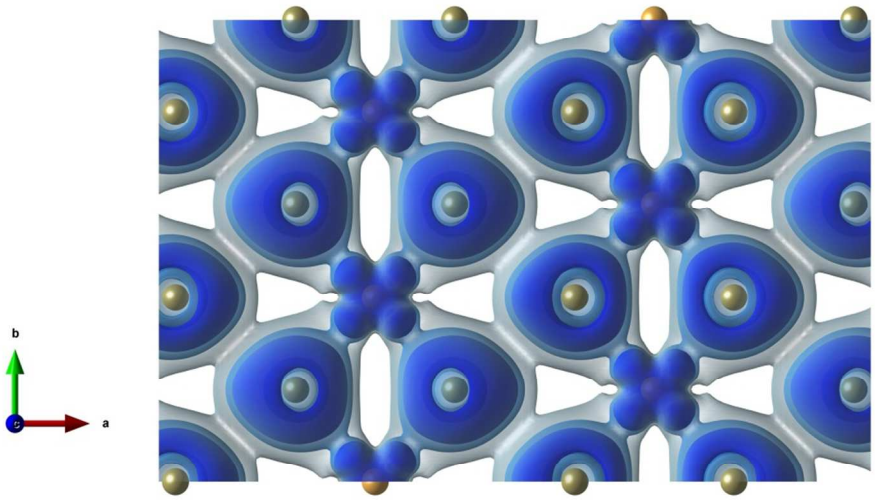

FigureS4. Electron density contour map of the planar [$AuTe_2$] layer.

V. Brillouin Zone of [Pb_2BiS_3][$AuTe_2$]

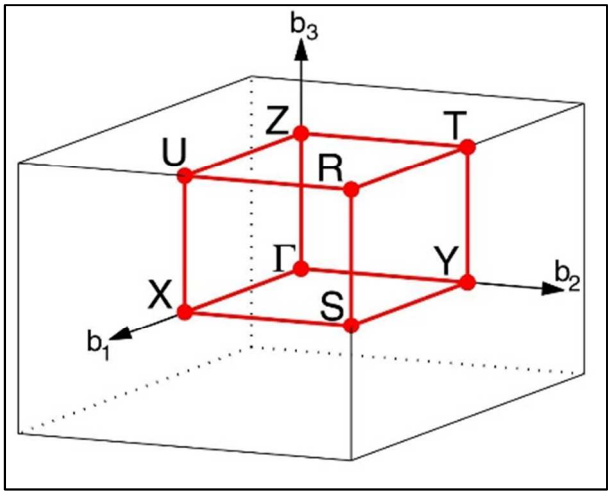

Figure S5. Brillouin Zone of [Pb_2BiS_3][$AuTe_2$]

VI. Optical images of bulk and exfoliated crystals

Bulk crystals were exfoliated on 300nm SiO_2/Si substrate using the standard scotch tape method. A sea-green color of thin flakes under visible light can be observed in different samples. This sea-green pigment is clearly different with the golden color of bulk crystals, indicating the flakes are sufficiently thin to induce optical properties change. The thickness can be qualitatively estimated using the well-determined thickness-color relation [S5] of 2D material MoS_2, although the electronic properties of these two materials are different. The sea-green pigment indicates 10 nm thickness approximately, corresponding to 10 unit cell of $[Pb_2BiS_3][AuTe_2]$ stacking along the *c*-axis. The dark shadow at the edges of the exfoliated crystals could be induced by the pixel limit of optical microscope or caused by the slightly tilted microscope sample stage.

Further efforts to pursue monolayer and precise determination of the nano-flake thickness using atomic force microscopy will be conducted in the future. Nevertheless, the color variation with sample thickness strongly indicates a tendency to form monolayer or few layers.

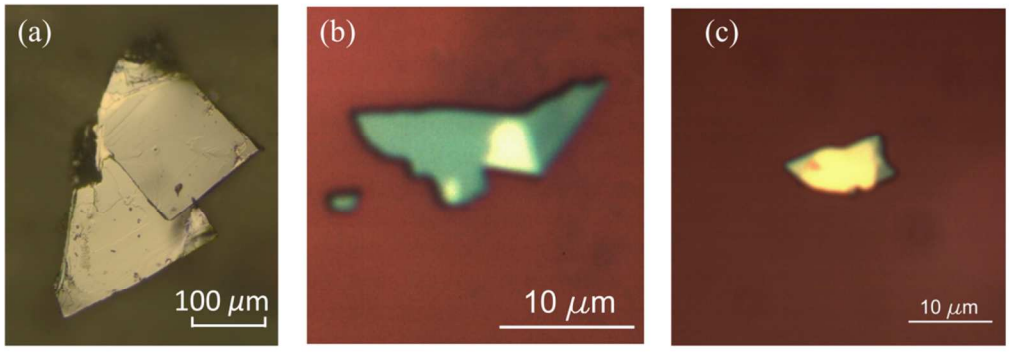

Figure S6. Optical images of bulk crystal, exfoliated nano-flake #1 and #2 (from left to right).

VII. Interlayer distance of $[Pb_2BiS_3][AuTe_2]$, MoS_2, $Bi_2Sr_2CaCu_2O_8$ and graphite

The nearest interlayer distance between building blocks [Pb_2BiS_3] and [$AuTe_2$] is 3.6709Å. The length of van der Waals bonds of MoS_2 and graphite are 3.4881 Å and 3.3705 Å, respectively [S6, S7]. For high temperature superconductor $Bi_2Sr_2CaCu_2O_8$, crystal cleavage happens between the two [Bi_2O_2] planes, shown in Figure S7(c). The nearest bond length between the two [Bi_2O_2] planes is 3.4084 Å [S8]. Therefore, the interlayer coupling strength of [Pb_2BiS_3][$AuTe_2$] should be comparable to these notable 2D materials which enable monolayers.

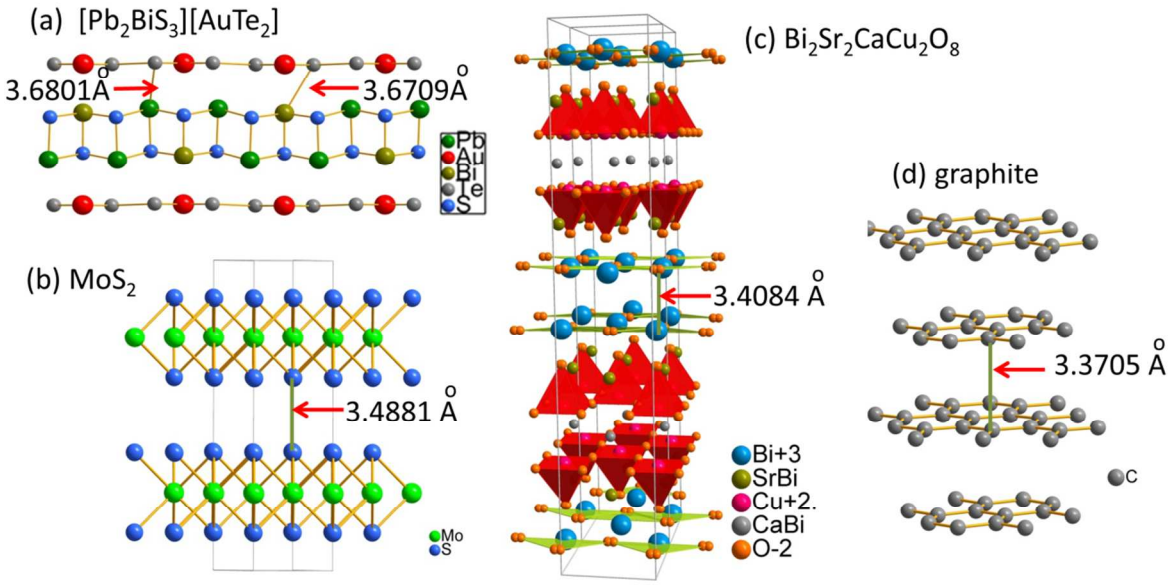

Figure S7. The interlayer distance of [Pb_2BiS_3][$AuTe_2$], MoS_2, $Bi_2Sr_2CaCu_2O_8$ and graphite.

References

[S1] Ziman, J. M. *Electrons and Phonons*, Oxford University Press, **1967**.

[S2] Wilson J. A.; Yoffe, A. D. *Adv. Phys.* **1969**, 18, 193−335.

[S3] Fang, L.; Wang, Y.; Zou, P. Y.; Tang, L.; Xu, Z.; Chen, H.; Dong, C.; Shan, L.; Wen, H. H. *Phys. Rev. B* **2005**,72, 014534.

[S4] Ashcroft, N. W.; Mermin, D. N. *Solid State Physics*, Saunders College Publishing, **1976**.

[S5] Li, H.; Wu, J.; Huang, X.; Lu, G.; Yang, J.; Lu, X.; Xiong, Q.; Zhang, H. *ACS Nano* 2013, 7, 10344−10355.

[S6] Dickinson, R.G.; Pauling, L. *J. Am. Chem. Soc.* **1923**, 45, 1466-1471.

[S7] Nixon, D. E.; Parry, G. S.; Ubbelohde, A. R. *Proc. R. Soc. London, Ser. A: Math. Phys. Sci.* **1966**, 291, 324-339.

[S8] Gao, Y.; Coppens, P.; Cox, D. E.; Moodenbaugh, A. R. *Acta Crystallogr., Sect. A: Found. Crystallogr.* **1993**, 49, 141-148.